

A Deep Learning Framework for Medium-Term Covariance Forecasting in Multi-Asset Portfolios*

Pedro Reis,[†] Ana Paula Serra[‡] and João Gama[§]

*This work was carried out within the scope of the research project funded by Fundação para a Ciência e a Tecnologia, grant number 2023.01070.BD.

[†]University of Porto, School of Economics and Management and Center for Economics and Finance (cef.up), R. Dr Roberto Frias 46, 4200-464 Porto, Portugal; and INESC TEC, Campus da Faculdade de Engenharia da Universidade do Porto, R. Dr. Roberto Frias, 4200-465 Porto, Portugal. Email: pdreis1988@gmail.com

[‡]University of Porto, School of Economics and Management and Center for Economics and Finance (cef.up), R. Dr Roberto Frias 46, 4200-464 Porto, Portugal.

[§]INESC TEC, Campus da Faculdade de Engenharia da Universidade do Porto, R. Dr. Roberto Frias, 4200-465 Porto, Portugal.

Abstract

Accurate covariance forecasting is central to portfolio allocation, risk management, and asset pricing, yet many existing methods struggle at medium-term horizons, where shifting market regimes and slower dynamics predominate. We propose a deep learning framework that combines three-dimensional convolutional neural networks, bidirectional long short-term memory layers, and multi-head attention to capture complex spatio-temporal dependencies. Using daily data on 14 exchange-traded funds from 2017 through 2023, we find that our model reduces Euclidean and Frobenius distance metrics by up to 20% relative to classical benchmarks (e.g., shrinkage and GARCH approaches) and remains robust across distinct market regimes. Our portfolio experiments demonstrate significant economic value through lower volatility and moderate turnover. These findings highlight the potential of advanced deep learning architectures to improve medium-term covariance forecasts, offering practical benefits for institutional investors and risk managers.

Keywords: Covariance Matrix Forecasting, Deep Learning, Portfolio Optimisation, Medium-Term Horizons, Financial Markets.

JEL codes: C45, G11, G17.

1 Introduction

Covariance matrix estimation is central in modern finance. It influences portfolio construction, risk management, and asset pricing models. [Markowitz \(1952\)](#) introduced mean-variance optimisation, highlighting how correlation among assets shapes the risk-return trade-off. Beyond portfolio choice, covariance estimation underpins factor-based models, hedging strategies, and even debates on market efficiency, where accurate correlation forecasts can drive risk control and potential out-performance.

Early studies found that even simple correlation structures could improve capital allocation. For instance, [Elton and Gruber \(1973\)](#) suggested using constant-correlation estimates over historical windows for a decade. Their work showed that stable or slowly changing correlation patterns can help avoid distortions caused by transient market fluctuations.

Over time, multiple research strands have focused on short-horizon covariance forecasts. High-frequency datasets, such as intraday prices, enable detailed volatility analyses, often using generalised autoregressive conditional heteroskedasticity (GARCH) based models. Constant ([Bollerslev, 1990](#)) and dynamic conditional correlation ([Engle, 2002](#)) specifications remain common benchmarks, although [Symitsi et al. \(2018\)](#) argue that little fundamental progress has been made recently. Extensions include applying the heterogeneous autoregressive model ([Corsi, 2009](#)) in a multivariate setting through Cholesky decomposition¹ ([Chiriac and Voev, 2011](#)). However, the Cholesky decomposition models outperform DRD-based² ([Bollerslev et al., 2018](#)).

However, GARCH-type approaches struggle with large cross-sections, falling prey to the curse of dimensionality ([Robert F. Engle and Wolf, 2019](#)). Tools like principal component analysis and random matrix theory ([Ledoit and Wolf, 2003](#); [Laloux et al., 2000](#)) have been effective for large datasets. Recent advances, such as dynamic conditional correlation with nonlinear shrinkage ([Robert F. Engle and Wolf, 2019](#)), perform well overall, as per [De Nard et al. \(2024\)](#). Still, most of these methods focus on very short-term horizons, often just one step ahead or one day ahead, and

¹Cholesky decomposition is a method that breaks down a positive definite matrix into the product of a lower triangular matrix and its transpose.

²Dynamic Relationship/Dependence (DRD) models refer to time-varying models that separate covariance into volatility and correlation components forecasts.

rely on high-frequency data.

Long-horizon forecasts matter for institutional investors like pension funds and endowments, which rebalance portfolios over weeks or months. Moreover, high-frequency data are not always public or cost-effective, making the short-horizon focus less relevant for these institutions. Furthermore, slow-moving trends, such as equity–bond correlation shifts, can be overlooked if one relies solely on high-frequency econometric models. [Sandoval and Franca \(2012\)](#) highlights how regime shifts or significant structural changes often go undetected in classical specifications, raising the risk of large drawdowns and poor capital allocation.

For longer-term horizons, naive, shrinkage, and factor models are more common ([Ledoit and Wolf, 2004](#); [De Nard et al., 2022](#)). Naive approaches assume that recent covariance estimates strongly predict future covariances as they follow a Markov process. At the same time, shrinkage techniques blend the sample covariance matrix with structured targets to reduce noise, particularly when the cross-section of assets is large ([Ledoit and Wolf, 2022](#)). Factor models can provide more insight but may not generalise well across diverse portfolios, especially when markets are affected by many different factors. These methods are typically stable but can underperform when major shifts occur.

In recent years, there has been a surge in machine learning methods that can handle nonlinearities and high dimensionality. [Gu et al. \(2020\)](#) and [Kim et al. \(2023\)](#) use techniques like random forests, support vector machines, and generative adversarial networks, while [Zhang et al. \(2024\)](#) applies graph neural networks to capture volatility spillovers for covariance matrix forecast. However, most of these solutions still emphasise short-term horizons.

Attention mechanisms ([Vaswani et al., 2017](#)) offer a promising direction by weighting key observations more heavily. Some studies apply these techniques in finance but still focus on short-horizon tasks ([Nazareth and Ramana Reddy, 2023](#); [Olorunnimbe and Viktor, 2023](#)). In principle, attention-based models could capture the slow-moving, cyclical factors and abrupt shifts that define medium- and long-horizon covariance forecasts, realising this potential. However, it requires integrating sophisticated data-driven architectures with the economic logic of excess returns.

Recent efforts to extend these approaches to multi-asset portfolios have been limited. While many studies handle large cross-sections of stocks or focus on single-asset classes such as equities ([Reis et al., 2024](#)), fewer examine the combined dynamics across multiple asset classes in an integrated framework. However, institutional investors routinely diversify across equities, bonds, alternatives, and derivatives, underscoring the need for robust, multi-asset covariance forecasting

models. In particular, capturing time-varying cross-asset correlations over medium-term horizons is a non-trivial challenge that remains under-explored in much of the existing literature.

Two key research gaps remain. First, most existing studies focus on short- or long-term horizons, leaving a relative void in medium-term covariance forecasting. This gap is particularly salient for multi-asset portfolios, where cross-asset correlations over multi-week or multi-month windows can significantly influence asset allocation and risk management (De Nard et al., 2021). Second, there is limited empirical evidence on whether using *raw* returns versus *excess* returns leads to systematically different covariance forecasts, especially over these medium-term horizons. Economic theory suggests that risk premiums and the underlying drivers of asset co-movements could be more accurately captured through *excess* returns. However, most machine learning and econometric approaches mostly default to *raw* returns.

Our study addresses these gaps by focusing on medium-term covariance forecasts in a multi-asset setting. Specifically, we propose a novel deep learning (DL) model that captures spatio-temporal correlations while remaining robust to structural changes. We benchmark against classical methods (naive, shrinkage, GARCH, and dimensional reduction) and demonstrate consistent gains in forecast accuracy under diverse market environments from 2017 to 2023. Our main contributions are as follows:

- We present an integrated 3D-convolution neural network (CNN) and bidirectional long-short-term memory (LSTM) architecture with multi-head attention that improves medium-term forecasting accuracy.
- We compare different return-processing specifications (including the treatment or omission of risk-free rates) and show that the proposed approach preserves its predictive edge.
- We evaluate the economic value of our forecasts in a global minimum-variance (GMV) portfolio, demonstrating significant variance reduction and stable turnover.

The rest of the paper is structured as follows. Section 2 introduces the benchmark methods and our DL model. Section 3 presents the main empirical findings. Section 4 reports robustness checks. Section 5 explores implications for portfolio management. Finally, Section 6 concludes.

2 Methodology

Let \mathbf{r}_t denote the N -dimensional row vector of excess daily returns for N assets at time t . Assuming time-varying mean excess returns, \mathbf{r}_t can be expressed as follows:

$$\mathbf{r}_t = \boldsymbol{\mu}_t + \mathbf{e}_t \quad (1)$$

where $\boldsymbol{\mu}_t$ is the N -dimensional vector of rolling means of the excess daily returns, and \mathbf{e}_t is the i.i.d. error terms with a normal distribution within each rolling window:

$$\mathbf{e}_t \sim N(\mathbf{0}, \boldsymbol{\Sigma}_t) \quad (2)$$

Although empirical evidence suggests financial returns often exhibit heavy tails and non-zero skewness (Cont, 2001), we adopt the normality assumption because it is standard in many benchmark models (e.g., GARCH-based correlation models and Ledoit–Wolf shrinkage). However, we acknowledge that alternative distributions (e.g., Student- t innovations, mixture models, or those explicitly modelling tail dependence) may better capture extreme events and skewness in practice³ (Hansen, 1994; Harvey, 1997).

The rolling mean $\boldsymbol{\mu}_t$ and rolling standard deviation $\boldsymbol{\sigma}_t$ at time t are calculated using a window of size F as follows:

$$\boldsymbol{\mu}_t = \frac{1}{F} \sum_{k=t-F+1}^t \mathbf{r}_k \quad (3)$$

$$\boldsymbol{\sigma}_t^2 = \frac{1}{F-1} \sum_{k=t-F+1}^t (\mathbf{r}_k - \boldsymbol{\mu}_t) \odot (\mathbf{r}_k - \boldsymbol{\mu}_t) \quad (4)$$

where \odot denotes the element-wise product. Therefore, the realised covariance matrix ($\boldsymbol{\Sigma}_t$) is an

³Extending our DL framework to accommodate such heavy-tailed or asymmetric distributions is an area for future research. Nevertheless, our empirical results in subsequent sections suggest that even a normality-based design can significantly enhance covariance forecasts, given the robustness of the data-driven layers in handling complex, nonlinear dependencies.

$N \times N$ matrix with each element calculated as:

$$Cov_t(\mathbf{r}_i, \mathbf{r}_j) = \frac{1}{F-1} \sum_{k=t-F+1}^t (r_{i,k} - \mu_{i,t})(r_{j,k} - \mu_{j,t}) \quad (5)$$

Our goal is to estimate the conditional covariance matrix of the asset returns for the next F days based on the information available at time t :

$$\widehat{\Sigma}_{t+1:t+F} = Cov(\mathbf{r}_{t+1}, \mathbf{r}_{t+2}, \dots, \mathbf{r}_{t+F} | \mathcal{F}_t) \quad (6)$$

where \mathcal{F}_t is the sigma-algebra representing all the information available at time t .

To estimate $\widehat{\Sigma}_{t+1:t+F}$, we compare naive and other benchmark models found in the literature alongside our proposed model. A description of each model is shown below.

2.1 Naïve (NA)

A naive covariance forecasting approach is based on the lagged realised covariance. This model assumes that covariance is a Markov process, so the covariance matrix of the previous period is highly informative about the future covariance matrix. Under this model:

$$\widehat{\Sigma}_{t+1:t+F} = \Sigma_{t-F:t} \quad (7)$$

This forecasting method is as simple as possible as it requires no optimisation.

2.2 Naïve full sample(NA^F)

Another naïve technique is to use the full sample instead of the rolling covariance matrix as our estimator.

$$\widehat{\Sigma}_{t+1:t+F} = \Sigma \quad (8)$$

where Σ is the covariance matrix of our sample up until t .

2.3 Exponential Weighted Moving Average (EWMA)

The EWMA employs exponentially decaying weights for the covariance matrix. The covariance matrix in the EWMA model is recursively computed as follows:

$$\widehat{\Sigma}_{t+1:t+F} = (1 - \eta)\mathbf{e}_t\mathbf{e}_t' + \eta\Sigma_{t-F:t} \quad (9)$$

where \mathbf{e}_t is the N-dimensional vector of the error terms of all assets from Eq. (1), at time t , and η acts as a decay factor, confined within the range $[0,1]$, dictating the rate at which the weights on past observations decrease. This factor has been approximated to be around 0.94 (J.P.Morgan, 1996).

2.4 Ledoit and Wolf (LW)

The LW shrinkage (Ledoit and Wolf, 2004) is a robust statistical model that combines the sample covariance matrix with a structured target matrix, improving estimation accuracy by reducing the impact of estimation error due to high dimensionality and limited sample size. The LW shrinkage estimator is given by:

$$\widehat{\Sigma}_{t+1:t+F} = \rho\mathbf{T} + (1 - \rho)\Sigma_{t-F:t} \quad (10)$$

where $\mathbf{T} = \frac{\text{Tr}(\Sigma_{t-F:t})}{N} \times \mathbf{I}$ is the target matrix, with \mathbf{I} being the identity matrix and $\text{Tr}(\Sigma_{t-F:t})$ representing the sum of the diagonal elements of the sample covariance matrix. The shrinkage coefficient ρ is optimally determined to minimise the mean squared error between the estimated and true covariance matrices:

$$\rho = \frac{\sum_{i \neq j} \text{Var}(\sigma_{i,j})}{\sum_{i \neq j} (\sigma_{i,j} - t_{i,j})} \quad (11)$$

where $\sigma_{i,j}$ are the elements of the sample covariance matrix and $t_{i,j}$ are the elements of the target matrix \mathbf{T} .

2.5 Ledoit and Wolf full sample (LW^F)

Similarly to the NA^F model, we employed a full sample of Ledoit and Wolf (2004) as a shrinkage model.

$$\widehat{\Sigma}_{t+1:t+F} = \rho\mathbf{T} + (1 - \rho)\Sigma \quad (12)$$

2.6 Constant Conditional Correlations (CCC)

The CCC model, introduced by [Bollerslev \(1990\)](#), assumes that asset correlations remain constant over time while variances evolve dynamically according to a GARCH process based on a one-step forecast. However, since investment funds and risk managers typically rebalance portfolios over extended horizons, such as monthly or quarterly, a one-step forecast is insufficient for practical decision-making ([De Nard et al., 2022](#)).

To extend the model to a multi-step forecasting framework, we follow the methodology of [Baillie and Bollerslev \(1992\)](#), defining the F -step ahead conditional covariance forecast as:

$$\hat{\Sigma}_{t+1:t+F} = \frac{1}{F} \sum_{f=1}^F \mathbf{D}_{t+f} \mathbf{R} \mathbf{D}_{t+f}, \quad (13)$$

where $\mathbf{D}_{t+f} = \text{diag}(\sqrt{h_{11,t+f}}, \sqrt{h_{22,t+f}}, \dots, \sqrt{h_{NN,t+f}})$ is the diagonal matrix of forecasted conditional volatilities for horizon f and \mathbf{R} the conditional correlation matrix. The multi-step averaging approach used in Eq. (13) was introduced by [De Nard et al. \(2021\)](#) to provide a more stable covariance forecast over the rebalancing period. The $h_{ii,t}$ series is modelled using univariate GARCH(1,1) processes:

$$h_{ii,t+f} = \sum_{j=0}^{f-1} \omega_i (\alpha_i + \beta_i)^j + (\alpha_i + \beta_i)^f h_{ii,t}, \quad (14)$$

where $\omega_i, \alpha_i, \beta_i$ are the estimated GARCH parameters.

The conditional correlation matrix \mathbf{R} is assumed to be constant over time calculated through the standardised residuals, which are defined as:

$$z_{i,t} = \frac{e_{i,t}}{\sqrt{h_{ii,t}}}, \quad (15)$$

where $e_{i,t}$ are the residuals of the return series, which are used to estimate the conditional correlation matrix.

2.7 Dynamic Conditional Correlations (*DCC*)

The *DCC* model of Engle (2002) extends the *CCC* model by allowing correlations to vary over time while retaining the GARCH framework for variances. This is achieved by replacing the constant correlation matrix in Eq. (13) with a dynamic correlation matrix \mathbf{R}_t .

To accommodate multi-step forecasting for practical portfolio management, we follow the methodology of Engle and Sheppard (2001). The F -step ahead conditional covariance forecast is:

$$\widehat{\Sigma}_{t+1:t+F} = \frac{1}{F} \sum_{f=1}^F \mathbf{D}_{t+f} \mathbf{R}_{t+f} \mathbf{D}_{t+f}, \quad (16)$$

where \mathbf{D}_{t+f} is defined as in Eq. (13), and \mathbf{R}_{t+f} is the f -step ahead forecast of the dynamic conditional correlation matrix. The multi-step forecast for the correlation matrix is computed as follows:

$$\mathbf{R}_{t+f} = \sum_{j=0}^{f-1} (1 - \alpha - \beta) \overline{\mathbf{Q}} (\alpha + \beta)^j + (\alpha + \beta)^f \mathbf{R}_t, \quad (17)$$

where $\overline{\mathbf{Q}}$ is the unconditional correlation matrix, and $\alpha + \beta < 1$ ensures stationarity. The parameters α and β control the persistence of the dynamic correlations.

The conditional correlation matrix \mathbf{R}_t evolves over time according to:

$$\mathbf{R}_t = \mathbf{V}_t^{-1} \mathbf{Q}_t \mathbf{V}_t^{-1} \quad (18)$$

$$\mathbf{Q}_t = (1 - \alpha - \beta) \overline{\mathbf{Q}} + \alpha \mathbf{z}_{t-1} \mathbf{z}'_{t-1} + \beta \mathbf{Q}_{t-1}, \quad (19)$$

where $\mathbf{V}_t = \text{diag}\{\sqrt{q_{11,t}}, \sqrt{q_{22,t}}, \dots, \sqrt{q_{NN,t}}\}$ ensures that \mathbf{R}_t remains a proper correlation matrix. The standardised residuals \mathbf{z}_t are defined as in Eq. (15), and $\overline{\mathbf{Q}}$ is estimated from historical standardised residuals.

2.8 Nonlinear Shrinkage Dynamic Conditional Correlations (*DCC^{NL}*)

One recent extension is the *DCC^{NL}* model from De Nard et al. (2022). The covariance forecast in the *DCC^{NL}* model follows the same structure as in Eq. (16), but now with a shrinkage-improved correlation matrix ($\overline{\mathbf{Q}}$). They apply the nonlinear shrinkage method of Ledoit and Wolf (2020), which optimally shrinks the eigenvalues of the sample covariance matrix towards a better-

conditioned target matrix. This procedure ensures that the estimated correlation matrix remains positive, definite, and well-conditioned, even in high-dimensional settings.

Given a sample correlation matrix Υ , the optimal nonlinear shrinkage estimator adjusts its eigenvalues as follows. Let Υ have the eigendecomposition:

$$\Upsilon = \mathbf{U}\mathbf{\Lambda}\mathbf{U}^\top, \quad (20)$$

where \mathbf{U} is the matrix of eigenvectors and $\mathbf{\Lambda} = \text{diag}(\lambda_1, \lambda_2, \dots, \lambda_N)$ is the diagonal matrix of eigenvalues. The nonlinear shrinkage transformation replaces $\mathbf{\Lambda}$ with a shrinkage-transformed version $\mathbf{\Lambda}^*$:

$$\Upsilon^* = \mathbf{U}\mathbf{\Lambda}^*\mathbf{U}^\top \quad (21)$$

where the optimally shrunk eigenvalues λ_i^* are computed using the oracle nonlinear shrinkage function:

$$\lambda_i^* = \lambda_i \frac{1}{(\pi c \lambda_i f(\lambda_i))^2 + (1 - c - \pi c \lambda_i H_f(\lambda_i))^2} \quad (22)$$

where $f(\lambda_i)$ is the sample spectral density estimator, $H_f(\lambda_i)$ is the Hilbert transform of the spectral density, and $c = \frac{N}{T}$ is the limiting concentration ratio of the covariance matrix.

The sample spectral density function $f(x)$ is estimated using a kernel-based density estimator, ensuring uniform consistency. The Hilbert transform $H_f(x)$ is computed using the principal value integral, which corrects for eigenvalue bias induced by sampling variability.

The shrunk correlation matrix (Υ^*) is then used as the input for the *DCC* process in Eq. (18).

2.9 Principal Component Analysis (PCA)

As noted by [Ledoit and Wolf \(2003\)](#), empirical results show the usefulness of PCA in covariance matrix estimation. The PCA is computed as follows:

$$\widehat{\Sigma}_{t+1:t+F} = \mathbf{U}\mathbf{\Lambda}\mathbf{U}^\top \quad (23)$$

To ensure we capture most of the information, we retain only the first k principal components

that account for at least 95% of the total variance. This is mathematically expressed as:

$$\sum_{i=1}^k \lambda_i \geq 0.95 \sum_{i=1}^N \lambda_i \quad (24)$$

The final forecasted covariance matrix is then approximated as:

$$\hat{\Sigma}_{t+1:t+F} \approx \mathbf{U}_k \mathbf{\Lambda}_k \mathbf{U}_k^\top \quad (25)$$

2.10 Random Matrix Theory (RMT)

RMT (Laloux et al., 2000) is built upon the *PCA* where the upper (ζ_+) and lower (ζ_-) bound of the eigenvalues are calculated using the Marchenko-Pastur distribution. These bounds are calculated as:

$$\lambda_+ = \left(1 + \frac{1}{\sqrt{q}}\right)^2, \quad \lambda_- = \left(1 - \frac{1}{\sqrt{q}}\right)^2 \quad (26)$$

where $q = T/N$ is the ratio of the window size to the number of assets. Eigenvalues within these bounds are dominated by noise, while eigenvalues outside the bounds represent meaningful information.

$$\lambda_i^{\text{filtered}} = \begin{cases} \lambda_i & \text{if } \lambda_i > \lambda_+ \text{ or } \lambda_i < \lambda_- \\ \frac{\lambda_+ + \lambda_-}{2} & \text{otherwise} \end{cases} \quad (27)$$

This filtering process removes noise and retains only the significant components of the covariance matrix. The cleaned covariance matrix is reconstructed by multiplying the filtered eigenvalues with their corresponding eigenvectors:

$$\hat{\Sigma}_{t+1:t+F} = \mathbf{U} \mathbf{\Lambda}^{\text{filtered}} \mathbf{U}^\top \quad (28)$$

2.11 CNN with A-BiLSTM (CAB)

In our proposed model, each batch of input data is processed sequentially through all six stages, as described below.

2.11.1 Data Preprocessing

Let $\mathbf{B} = [\mathbf{D}_1, \mathbf{D}_2, \dots, \mathbf{D}_T]^\top$ be the time series data, where each $\mathbf{D}_t \in \mathbb{R}^{N \times N}$ represents the rolling covariance matrix, normalised, of N assets at time t).

It is essential to standardise the input features to facilitate efficient training and convergence of the *CAB* model. This transformation ensures that each feature has zero mean and unit variance, which is crucial for stabilising the training dynamics of neural networks.

We transform the data into overlapping sequences using a rolling window approach to capture temporal dependencies. Specifically, for a given lookback period L , the sequence creation process, at time t , can be expressed as:

$$\mathbf{S}_t = [\mathbf{D}_{t-L}, \mathbf{D}_{t-L+1}, \dots, \mathbf{D}_t]^\top \in \mathbb{R}^{L \times N \times N} \quad (29)$$

The input to the *CAB* model consists of sequences of scaled covariance matrices. Formally, let $\mathbf{S}_i \in \mathbb{R}^{L \times N \times N}$ denote the i -th sequence.

2.11.2 3D Convolutional Layer

Next, each sequence of covariance matrices is processed through a three-dimensional layer (Lecun et al., 1998). We use a 3D CNN to capture local spatio-temporal features, given that each rolling covariance matrix is an $(N \times N)$ grid, and the temporal dimension arises from stacking these grids over time. The 3D CNN filters can identify how subsets of assets interact and evolve over multiple past windows, offering a more flexible approach than linear assumptions.

By applying a convolution operation with a kernel size of $(ks \times ks \times ks)$, the same padding, and a stride equal to one, the CNN layer captures patterns within the data across different time steps and different dimensions of the covariance matrices. The transformation performed by the 3D convolutional layer on the input sequence of covariance matrices can be expressed as:

$$\mathbf{X}_{\text{conv}}(t, i, j) = \sum_{u=-\lfloor ks/2 \rfloor}^{\lfloor ks/2 \rfloor} \sum_{v=-\lfloor ks/2 \rfloor}^{\lfloor ks/2 \rfloor} \sum_{w=-\lfloor ks/2 \rfloor}^{\lfloor ks/2 \rfloor} \mathbf{W}(u, v, w) \cdot \mathbf{X}_{\text{rs}}(t + u, i + v, j + w) + b \quad (30)$$

where ks is the kernel size of the 3D Convolution, determining the dimensions of the receptive field across the temporal and spatial axes. $\mathbf{W}(u, v, w)$ represents the kernel weights, a learnable

parameter of size $C_{\text{out}} \times C_{\text{in}} \times k_s \times k_s \times k_s$, where C_{in} is the number of input channels, and C_{out} is the number of output channels. The input covariance matrices are reshaped to include a single channel, so $C_{\text{in}} = 1$. Additionally, the model outputs a single channel, meaning $C_{\text{out}} = 1$. Consequently, the weight tensor simplifies to $\mathbf{W} \in \mathbb{R}^{1 \times 1 \times k_s \times k_s \times k_s}$. $\mathbf{X}_{\text{rs}}(t + u, i + v, j + w)$ is the input sequence of covariance matrices reshaped to dimensions $1 \times L \times N \times N$. The term b denotes the bias added to the convolution result, which, with $C_{\text{out}} = 1$, is a single scalar, i.e., $b \in \mathbb{R}^1$. The indices u , v , and w iterate over all whole integers within the range $[-(k_s/2), (k_s/2)]$, centered around (t, i, j) , to compute local features. Finally, zero-padding is applied to ensure that the output dimensions match the input dimensions, preserving the temporal and spatial resolution of the covariance matrices.

Subsequently, the convolutional output is flattened ($\mathbf{X}_{\text{flattened}} \in \mathbb{R}^{L \times N^2}$) to transition from spatial to feature dimensions suitable for the LSTM layer. This reshaping consolidates the $N \times N$ covariance matrices into N^2 -dimensional feature vectors for each time step within the sequence.

2.11.3 Bidirectional LSTM (BiLSTM) Layer

Following the CNN, the flattened transformed sequences are fed into a layer configured with u layers and h_d hidden dimension. To understand the BiLSTM, it is essential first to grasp the fundamentals of a standard LSTM network (Hochreiter, 1997). Appendix A.1 provides more detailed information on how each LSTM cell works.

The BiLSTM enhances the standard LSTM by adding another layer that processes the input sequence in the reverse order. This bidirectional approach allows the model to have both forward and backward information about the sequence, making it more effective in capturing the context from past and future data points. Each sequence goes through u layers, i.e. the output of layer one serves as input for layer 2.

In our model, the BiLSTM first transforms the input sequence $\mathbf{X}_{\text{flattened}}$ of dimension $L \times N^2$ into an output sequence of dimension $L \times 2h_d$. The BiLSTM uses learnable parameters to map the N^2 features at each time step into a lower-dimensional hidden representation of size h_d . This transformation is achieved through linear transformations, where weights and biases are optimised during training. Then, the hidden states from both forward and backward pass across all layers, and time steps are concatenated to form a comprehensive hidden state matrix. This matrix captures information from all directions and spans the entire sequence of inputs. Each BiLSTM layer can be expressed as:

$$\mathbf{H}^o = \left[\mathbf{H}^{(1)}, \mathbf{H}^{(2)}, \dots, \mathbf{H}^{(h_d)} \right] \in \mathbb{R}^{L \times 2h_d} \quad (31)$$

where o represents the BiLSTM layer, for $o = 1, \dots, u$, and each $\mathbf{H}^{(l)}$ for $l = 1, 2, \dots, h_d$ is defined as:

$$\mathbf{H}^{(l)} = \begin{bmatrix} \vec{\mathbf{h}}_{t-L}^{(l)} & \overleftarrow{\mathbf{h}}_{t-L}^{(l)} \\ \vec{\mathbf{h}}_{t-L+1}^{(l)} & \overleftarrow{\mathbf{h}}_{t-L+1}^{(l)} \\ \vdots & \vdots \\ \vec{\mathbf{h}}_t^{(l)} & \overleftarrow{\mathbf{h}}_t^{(l)} \end{bmatrix} \in \mathbb{R}^{L \times 2} \quad (32)$$

The hidden dimension for each LSTM direction, denoted as h_d , results in a concatenated hidden state dimension of $2h_d$ at each time step.

The traditional BiLSTM outputs the last time step of the last layer. However, in our model, we use a similar approach to [Liu and Guo \(2019\)](#) methodology, meaning all time steps from the last layer (\mathbf{H}^u) are used as an input to our following steps. To mitigate overfitting and enhance the model’s generalisation capabilities, a Dropout Layer is applied to the BiLSTM output. This operation randomly zeroes a fraction of the elements in \mathbf{H}^u with a probability of 20%, effectively regularising the model by preventing reliance on specific neurons during training. During our testing phase, this feature will be skipped.

2.11.4 Multi-Head Self-Attention Layer

Our next step is to apply a multi-head attention mechanism ([Vaswani et al., 2017](#)) to each hidden state of the last layer. The multi-head attention mechanism to refine the temporal dependencies captured in the sequence. For h_e attention heads, the input \mathbf{H}^u is used to compute the queries (\mathbf{Q}), keys (\mathbf{K}), and values (\mathbf{V}): $\mathbf{Q} = \mathbf{H}^u \mathbf{W}_q$, $\mathbf{K} = \mathbf{H}^u \mathbf{W}_k$, and $\mathbf{V} = \mathbf{H}^u \mathbf{W}_v$, where $\mathbf{W}_q, \mathbf{W}_k, \mathbf{W}_v \in \mathbb{R}^{2h_d \times 2h_d}$ are learnable parameters. The attention weights for each head are computed as follows:

$$\mathbf{Attention}(\mathbf{Q}_{\text{head}}, \mathbf{K}_{\text{head}}, \mathbf{V}_{\text{head}}) = \text{softmax} \left(\frac{\mathbf{Q}_{\text{head}} \mathbf{K}_{\text{head}}^\top}{\sqrt{d_k}} \right) \mathbf{V}_{\text{head}} \in \mathbb{R}^{L \times d_k} \quad (33)$$

where $d_k = \frac{2h_d}{h_e}$ scales the dot product to stabilise gradients and splits the features. Each head processes its respective portion of the features, which are concatenated to produce $\mathbf{A}_{\text{concat}} \in \mathbb{R}^{L \times 2h_d}$. The concatenated output is projected back to $\mathbf{A} = \mathbf{A}_{\text{concat}} \mathbf{W}_c \in \mathbb{R}^{L \times 2h_d}$ using a linear transforma-

tion.

The attention output is mean-pooled along the sequence dimension to condense the temporal information into a fixed-length representation:

$$\mathbf{a}_{\text{mean}} = \frac{1}{L} \sum_{t=1}^L \mathbf{A}_t \in \mathbb{R}^{1 \times 2h_d} \quad (34)$$

where \mathbf{A}_t is the t -th row of \mathbf{A} . This averaged context vector \mathbf{a}_{mean} encapsulates the overall information from the entire sequence. We then pass \mathbf{a}_{mean} through a fully connected layer to map it back to the covariance matrix space:

This averaged context vector \mathbf{a}_{mean} encapsulates the overall information from the entire sequence. We then pass \mathbf{a}_{mean} through a fully connected layer to map it back to the covariance matrix space:

$$\mathbf{y} = \mathbf{a}_{\text{mean}} \mathbf{W}_{\text{fc}} + \mathbf{b}_{\text{fc}} \in \mathbb{R}^{1 \times N^2} \quad (35)$$

where \mathbf{W}_{fc} and \mathbf{b}_{fc} are respectively the weight matrix and bias vector of the fully connected layer.

Because our pipeline stacks 3D Convolution, BiLSTM, and attention in succession, the final latent representation becomes highly abstract, making interpretability at each layer difficult. Consequently, we do not attempt to interpret the hidden states or attention weights in a domain sense.

2.11.5 Enforcing Symmetry and Positive Semi-Definiteness

The output vector \mathbf{y} is reshaped into a square matrix ($\mathbf{Y}_{\text{reshaped}} \in \mathbb{R}^{N \times N}$) to form the predicted covariance matrix.

The output matrix $\mathbf{Y}_{\text{reshaped}}$ may not necessarily be symmetric, a key property of covariance matrices. To enforce symmetry, we average the matrix with its transpose:

$$\mathbf{Y}_{\text{sym}} = \frac{\mathbf{Y}_{\text{reshaped}} + \mathbf{Y}_{\text{reshaped}}^{\top}}{2} \quad (36)$$

Then, we rescale the normalised output back to the original scale of the data, using the reverse process of Section 2.11.1 resulting in $\mathbf{Y}_{\text{sym}}^{\text{unscaled}}$.

Symmetry alone does not guarantee that $\mathbf{Y}_{\text{sym}}^{\text{unscaled}}$ is positive semi-definite, which is another requisite property of covariance matrices. To ensure positive semi-definiteness, we perform eigen-

value decomposition:

$$\mathbf{Y}_{\text{sym}}^{\text{unscaled}} = \mathbf{U}\mathbf{\Lambda}\mathbf{U}^\top \quad (37)$$

We then modify $\mathbf{\Lambda}$ by setting all negative eigenvalues to zero:

$$\mathbf{\Lambda}' = \text{diag}(\max(\lambda_i, 0)) \quad (38)$$

The positive semi-definite matrix is reconstructed as:

$$\mathbf{Y}_{\text{psd}} = \mathbf{U}\mathbf{\Lambda}'\mathbf{U}^\top \quad (39)$$

2.11.6 Shrinkage

While DL-based forecasts can learn intricate patterns, historical covariance may still convey valuable stability and continuity, particularly when the model is tested on data different from training. Therefore, our model's final step is incorporating a linear shrinkage from historical values in our predictions.

$$\mathbf{CAB} = \mathbf{Y}_{\text{psd}}\phi + \mathbf{\Sigma}_{t-F:t}(1 - \phi) \quad (40)$$

where \mathbf{CAB} is the final $N \times N$ matrix output, and ϕ is the shrinkage factor.

2.12 Evaluation metrics

We will use performance metrics consistent with previous literature (Symitsi et al., 2018; Bollerslev et al., 2018; Zhang et al., 2024) to check the models' performance. We consider the following loss functions to measure the average distance between predicted covariances and realised covariances matrices for the model comparisons:

$$\mathcal{L}_t^E = \sqrt{\text{vec}_{\text{Tri}}(\mathbf{\Sigma}_t - \hat{\mathbf{\Sigma}}_t)^\top \text{vec}_{\text{Tri}}(\mathbf{\Sigma}_t - \hat{\mathbf{\Sigma}}_t)} \quad (41)$$

$$\mathcal{L}_t^F = \sqrt{\text{Tr} \left[(\mathbf{\Sigma}_t - \hat{\mathbf{\Sigma}}_t)^\top (\mathbf{\Sigma}_t - \hat{\mathbf{\Sigma}}_t) \right]} \quad (42)$$

where \mathcal{L}_t^E represents the Euclidean distance between the $N(N + 1)/2$ dimensional vectorised version of the upper triangular of forecast covariances and ex-post realised covariances. \mathcal{L}_t^F is the

Frobenius distance between the two matrices, and Tr is the trace of a square matrix. All these functions measure losses. Therefore, lower values are preferred.

3 Empirical Results

We obtain our sample data from the Refinitiv Database, covering daily adjusted closing prices of 14 major ETFs that reflect equity and bond markets across diverse global sectors. These ETFs were selected to construct a multi-asset environment that includes equity sectors (e.g. technology, financials, industrials, consumer staples) and fixed-income exposures. Table 1 details the ETF’s information. To compute *excess* returns, we also retrieve from the Federal Reserve Economic Data the 1-month U.S. Treasury yield, treating it as a daily risk-free rate. Our sample runs from 1 January 2017 to 31 December 2023, totalling 1,760 trading days.

Table 1 – List of ETFs included in our research.

Name	Ticker	ISIN	Asset Class
iShares Global Tech ETF	IXN	US4642872919	Equity
iShares Global Financials ETF	IXG	US4642873339	Equity
iShares Global Consumer Discretionary ETF	RXI	US4642887453	Equity
iShares Global Industrials ETF	EXI	US4642887297	Equity
iShares Global Healthcare ETF	IXJ	US4642873255	Equity
iShares Global Consumer Staples ETF	KXI	US4642887370	Equity
iShares U.S. Real Estate ETF	IYR	US4642877397	Real Estate
iShares International Developed Real Estate ETF	IFGL	US4642884898	Real Estate
iShares Global Materials ETF	MXI	US4642886950	Equity
iShares Global Energy ETF	IXC	US4642873412	Equity
iShares Global Comm Services ETF	IXP	US4642872752	Equity
iShares Global Utilities ETF	JXI	US4642887115	Equity
iShares Core U.S. Aggregate Bond ETF	AGG	US4642872265	Fixed Income
iShares Core International Aggregate Bond ETF	IAGG	US46435G6724	Fixed Income

We split our dataset into a training period from 1 January 2017 to 31 December 2020 and a testing period covering 1 January 2021 to 31 December 2023. The testing sample thus comprises 753 trading days, encompassing a wide range of economic and market conditions. We identify three distinct market regimes within this testing window to examine whether our model responds robustly to varying interest-rate and equity-market environments. We designate the interval be-

tween 1 January 2021 and 2 January 2022 as the *First Bull Period* (Bull-1), typified by low yields on the risk-free asset and a generally stable equity market. We label the interval from 3 January 2022 to 12 June 2022 as the *Bear Period* (Bear), characterised by a steady rise in the risk-free rate and a drop of 20% or more in the S&P 500 from its last peak. Lastly, we classify the interval from 13 June 2022 to 31 December 2023 as the *Second Bull Period* (Bull-2), featuring persistently high interest rates but a renewed upswing in equity prices. This subdivision ensures that our out-of-sample evaluations capture both low- and high-rate market phases and a bear-market regime, offering a comprehensive test of the model’s ability to adapt to evolving financial landscapes.

During the training period, we minimise the Frobenius distance (Eq. 42) to select hyperparameters. We use *Optuna* (Akiba et al., 2019) for hyperparameter selection. Appendix A.2 shows the grid search table. Specifically, we split the training dataset into a model-fitting subset (80%) and a validation subset (20%) to identify optimal settings under a forecast horizon (F) of 20 days. We adopt the Adam optimiser over 100 epochs, using a batch size of 128 and a learning rate of 10^{-4} . For the neural-network-based *CAB* model, we use a lookback window (L) of 100 days. We set the 3D convolution kernel size (ks) to five; the BiLSTM has 128 hidden dimensions (hd) across seven stacked layers (u), and the multi-head attention uses 16 heads (he). Finally, we apply a shrinkage factor of 0.8 (ϕ) when combining the DL output with the most recent historical covariance.

We conduct a rolling estimation procedure to simulate live conditions. Each new trading day t in the test set triggers an online update of our DL model, incorporating all data up through day t . This design ensures that the forecasts mimic a real-world trading environment, where only up-to-date historical data is available at each decision point.

Table 2 reports the average Euclidean (\mathcal{L}^E) and Frobenius (\mathcal{L}^F) distances between forecasted and realised covariance matrices for all models over the entire testing period (2021–2023)⁴. GARCH models (*CCC* and *DCC*) and *EWMA* perform relatively well as they adapt faster to structural changes in the covariance matrices. However, our model (*CAB*) yields the lowest errors in both metrics, outperforming classical benchmarks. Dimensional reduction models perform inadequately as we only use 14 assets.

To solidify our findings, we analysed the 10 models with 753 paired samples for the Euclidean

⁴Bold and underlined numbers represent the lowest and the second lowest values, respectively.

Table 2 – Average Euclidean (\mathcal{L}^E) and Frobenius (\mathcal{L}^F) distances ($\times 10^5$) for whole the testing period (1 January 2021 to 31 December 2023).

	\mathcal{L}^E	\mathcal{L}^F
<i>NA</i>	53.526	82.020
<i>NA^F</i>	52.713	80.987
<i>EWMA</i>	49.111	75.349
<i>LW</i>	49.772	76.514
<i>LW^F</i>	68.136	103.363
<i>CCC</i>	48.568	75.198
<i>DCC</i>	<u>48.268</u>	<u>74.716</u>
<i>DCC^{NL}</i>	51.621	79.079
<i>PCA</i>	54.348	83.154
<i>RMT</i>	54.145	82.915
<i>CAB</i>	38.312	58.923

and Frobenius distances following Demsar (2006) frequentist methodology. The significance level is $\alpha = 0.050$ for all tests here forward. We rejected the null hypothesis that the population is normal for all the populations ($p < 0.01$ for all models in both distances). Therefore, we assume that not all populations are normal.

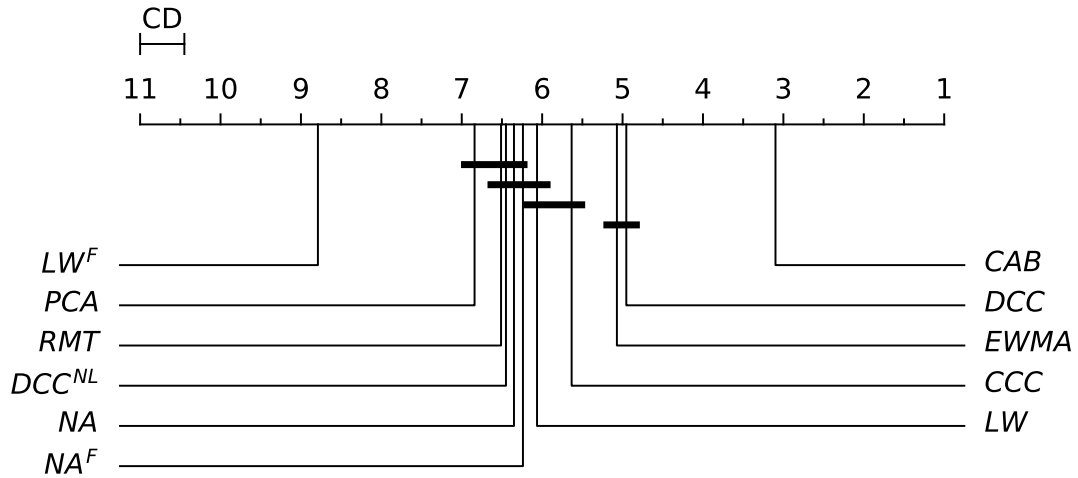
Because we have more than two populations and the populations are not normal, we use the non-parametric Friedman test as an omnibus test to determine if there are any significant differences between the median values of the populations. We use the post-hoc Nemenyi test to infer which differences are significant. Differences between populations are significant if the difference in the mean rank is greater than the critical distance $CD=0.494$ of the Nemenyi test.

We reject the Friedman test’s null hypothesis, which states that there is no difference in the central tendency of the populations. Therefore, we assume that there is a statistically significant difference between the central tendencies of the populations. Figure 1 shows the post-hoc Nemenyi test critical distance between groups. Our model reports statistically better results than the benchmark models.

Table 3 presents the average distance metrics for the testing period across three market regimes: Bull-1, Bear, and Bull-2. Overall, the *CAB* model consistently outperforms all benchmarks.

While all models experience a decrease in accuracy during the turbulent Bear regime, the *CAB* approach exhibits notable robustness. In particular, during the Bull-2 period, characterised by

(a) Upper Triangular Euclidean distance



(b) Frobenius distance

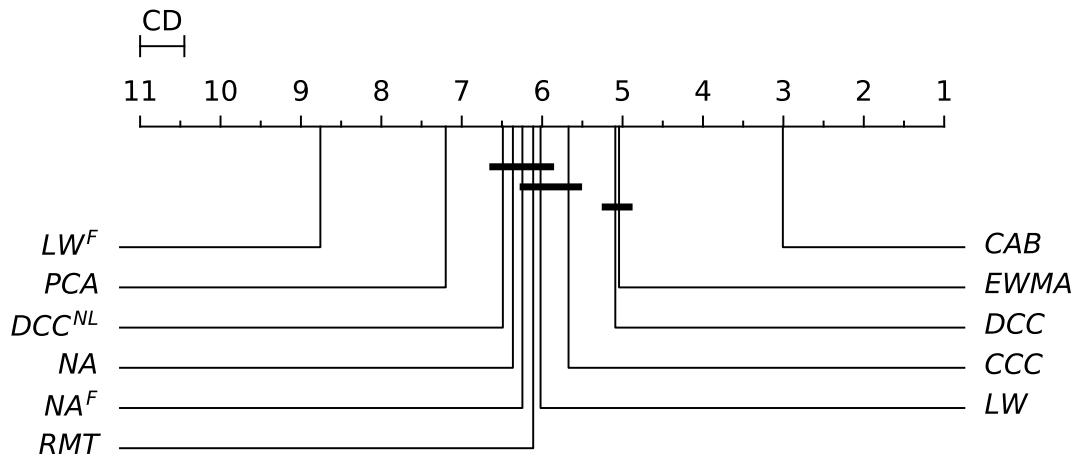


Figure 1 – Critical distance diagrams for the post-hoc Nemenyi test.

Table 3 – Average Euclidean (\mathcal{L}^E) and Frobenius (\mathcal{L}^F) distances ($\times 10^5$) for different testing periods: Bull-1 (1 January 2021 to 2 January 2022), Bear (3 January 2022 to 12 June 2022), and Bull-2 (13 June 2022 to 31 December 2023).

	Bull-1		Bear		Bull-2	
	\mathcal{L}^E	\mathcal{L}^F	\mathcal{L}^E	\mathcal{L}^F	\mathcal{L}^E	\mathcal{L}^F
<i>NA</i>	36.937	56.621	89.891	137.868	53.709	82.252
<i>NA^F</i>	35.680	54.992	98.002	150.780	50.586	77.545
<i>EWMA</i>	31.754	<u>48.973</u>	<u>82.799</u>	<u>126.614</u>	50.574	77.549
<i>LW</i>	34.126	52.599	90.441	138.173	48.089	74.088
<i>LW^F</i>	63.288	94.759	93.189	143.636	63.989	97.222
<i>CCC</i>	<u>31.688</u>	49.784	88.106	134.902	48.017	74.316
<i>DCC</i>	33.516	52.166	84.745	130.345	<u>47.227</u>	<u>73.161</u>
<i>DCC^{NL}</i>	36.779	56.449	87.650	134.167	50.767	77.734
<i>PCA</i>	37.424	57.281	90.720	139.116	54.747	83.660
<i>RMT</i>	37.246	57.083	90.638	138.821	54.493	83.411
<i>CAB</i>	24.276	37.643	66.381	102.252	39.253	60.126

elevated interest rates and dynamic shifts in cross-asset relationships, integrating DL techniques with classical shrinkage enables *CAB* to adapt effectively to changing market conditions, thereby maintaining lower distance metrics.

Supplementary Nemenyi post-hoc tests confirm that the performance improvements observed with *CAB* are statistically significant. These tests provide further evidence that the model’s superior performance is not merely a result of sample-specific idiosyncrasies but reflects a robust ability to handle varying market regimes.

Moreover, these findings contribute to the literature on hybrid forecasting methods by demonstrating that blending modern DL with traditional econometric techniques can offer substantial gains in predictive accuracy, especially in periods of market stress. This robust performance under diverse macroeconomic conditions highlights the practical relevance of the *CAB* approach for risk management and strategic asset allocation.

4 Robustness analysis

4.1 Impact of Using Raw Returns vs. Excess Returns

One potential criticism of our model is that it may be overly tailored to *excess* returns, even though some classic optimisation frameworks (Markowitz, 1952) often use *raw* returns. We re-estimate our model without subtracting the risk-free rate to address this concern. All other model parameters remain identical to those described in Section 2, with the sole difference being that \mathbf{r}_t now represents the N -dimensional row vector of *raw* daily returns for N assets at time t .

Table 4 reports the performance of the various models under these *raw* returns assumptions. Our approach (*CAB*) continues outperforming all benchmarks across the entire sample and within individual market regimes, with statistically significant results based on the same post-hoc Nemenyi criteria used earlier. This finding directly informs our second research question about whether *raw* vs. *excess* returns lead to materially different covariance forecasts. When comparing Table 4 (*raw* returns) to Tables 2 and 3 (*excess* returns), the numerical magnitudes change slightly, but the rank order remains the same: *CAB* still produces the most accurate forecasts overall.

Our findings indicate that the advantage of our framework is not contingent on the choice between *excess* or *raw* returns, reaffirming its robustness to the presence or absence of the risk-free rate. Moreover, this consistency suggests that subtracting the risk-free rate over the medium-term horizon does not significantly alter the core structure of asset co-movements. Hence, even though economic theory posits that *excess* returns better capture risk premiums, our empirical results show that the forecasting edge of *CAB* holds across both *raw* and *excess* return specifications. In other words, our method retains its superior performance even when modelling raw returns, suggesting that its effectiveness does not hinge on subtracting the risk-free rate.

4.2 Varying Forecast Horizons

We also examine our model’s behaviour as the forecast horizon (F) varies. In the baseline analysis, $F = 20$ days are medium-term, but many institutional investors face different time horizons for risk management or asset allocation decisions. In line with our first research question regarding under-explored medium-term horizons, we extend F from 10 to 250 days, thus covering short, medium, and long horizons. To explore model performance across this range of settings, we evaluate both

Table 4 – Average Euclidean (\mathcal{L}^E) and Frobenius (\mathcal{L}^F) distances ($\times 10^5$) using *raw* returns for different testing periods: Overall (1 January 2021 to 31 December 2023), Bull-1 (1 January 2021 to 2 January 2022), Bear (3 January 2022 to 12 June 2022), and Bull-2 (13 June 2022 to 31 December 2023).

	Overall		Bull-1		Bear		Bull-2	
	\mathcal{L}^E	\mathcal{L}^F	\mathcal{L}^E	\mathcal{L}^F	\mathcal{L}^E	\mathcal{L}^F	\mathcal{L}^E	\mathcal{L}^F
<i>NA</i>	53.525	82.020	36.936	56.620	89.895	137.875	53.707	82.249
<i>NA^F</i>	52.486	80.668	34.913	53.883	98.623	151.717	50.462	77.372
<i>EWMA</i>	49.174	75.441	31.753	<u>48.972</u>	<u>82.798</u>	<u>126.613</u>	50.697	77.730
<i>LW</i>	49.771	76.512	34.125	52.598	90.442	138.174	48.087	74.085
<i>LW^F</i>	68.130	103.353	63.273	94.736	93.190	143.636	63.985	97.217
<i>CCC</i>	48.508	75.106	<u>31.599</u>	49.634	88.139	135.038	47.948	74.196
<i>DCC</i>	<u>48.232</u>	<u>74.661</u>	33.445	52.045	84.884	130.630	<u>47.161</u>	<u>73.050</u>
<i>DCC^{NL}</i>	51.604	79.051	36.691	56.305	87.856	134.535	50.731	77.664
<i>PCA</i>	54.348	83.153	37.423	57.280	90.724	139.123	54.745	83.657
<i>RMT</i>	54.144	82.914	37.245	57.081	90.643	138.829	54.491	83.408
<i>CAB</i>	36.663	56.518	22.807	35.673	62.036	96.406	38.273	58.441

excess (Table A2) and *raw* returns (Table A3).

Table A2 shows that our model consistently achieves the lowest average distance metrics across most forecast horizons. *CAB* remains among the top performers for shorter horizons ($F = 10$). However, it does not outperform GARCH-based models (*CCC* and *DCC*) and *EWMA*. These differences are not statistically different in the overall period, Bull-1 and Bull-2. During Bull-2, our model outperformed the benchmarks, and the results were statistically significant based on the post-hoc Nemenyi test.

For mid-term forecasting ($F = 40, 60, 90, 120, 180$) for both distances, the differences are statistically significant in all periods. Thus, our model consistently outperforms the benchmarks. Please note that GARCH models tend to underperform as the forecast horizon increases, while full data models (*NA^F* and *LW^F*) tend to diminish forecasting errors. Please note, while the *DCC^{NL}* was more recently designed for high dimensional matrices, it provides more stable forecasts based on eigenvalues than the classical *DCC*.

At the longest horizon ($F = 250$), *CAB* again excels in most periods. Besides showing a large difference between distances during the Bear period and Bull-1, the post-hoc Nemenyi test shows no statistical difference between our model and *NA^F* and *LW^F*, respectively. These results

suggest that more complex models capture slower-moving cross-asset dynamics effectively, while classical estimators remain competitive in certain regime-specific conditions. As anticipated, naive and shrinkage methods perform relatively well at the longer horizon. These patterns reinforce our first research question’s premise that medium-term horizons can benefit from sophisticated models and highlight instances where simpler approaches hold their own.

Turning to Table A3, we link our findings to the second research question: whether using *raw* or *excess* returns makes a systematic difference. Results show that the top-performing models remain consistent across all forecast horizons.

Once again, *CAB* tends to yield the strongest overall performance. Although it does not dominate at shorter horizons, it consistently ranks near the top, showing no statistical difference between our model and the top performers. All other differences are statistically significant. These results mirror the trends seen under *excess* returns, indicating that the performance edge of *CAB* does not hinge on subtracting the risk-free rate. Therefore, our DL approach remains robust even if practitioners opt for *raw* returns, common in certain classical optimisation frameworks. Our model performs better than the benchmarks for longer horizons ($F = 250$). However, the results are not statistically different from the second-performing models (NA^F and LW^F) for the Bull-1 and Bear periods, respectively.

These findings indicate that DL-based models can adapt effectively across different forecast windows. Across both dimensions, *CAB* shows a stable advantage, with only minor variations in extreme horizons.

5 Economic Value in Portfolio Management

Next, we investigate the economic importance of accurate covariance forecasts in a practical asset allocation framework. Specifically, we consider an investor allocating wealth among the ETFs specified in section 3, subject to a no-short-selling constraint. Such a constraint is common among regulated institutional investors (e.g., pension funds, mutual funds) that may face limits on leverage or short positions. We adopt daily, weekly, and monthly rebalancing intervals (Symitsi et al., 2018).

At each rebalancing date, the investor solves the GMV problem:

$$\min_{\mathbf{w}_t} \mathbf{w}_t^\top \widehat{\Sigma}_t \mathbf{w}_t \quad \text{subject to} \quad \mathbf{1}^\top \mathbf{w}_t = 1, \quad w_{i,t} \geq 0, \quad (43)$$

where \mathbf{w}_t is an $N \times 1$ vector of GMV portfolio weights, $\widehat{\Sigma}_t$ is the $N \times N$ forecast covariance from each model, and $\mathbf{1}$ is an $N \times 1$ vector of ones. Excluding expected returns from the optimisation allows us to isolate the impact of covariance forecasts (DeMiguel et al., 2009; Kourtis et al., 2012).

Using a rolling estimation window, we generate 11 portfolio strategies (one for each forecast model) plus an equally weighted ($1/N$) benchmark. After estimating $\widehat{\Sigma}_t$, we compute the GMV weights and hold them until the next rebalancing date. We then record the ex-post average portfolio return for each model (m) as:

$$\mathbf{r}_{t+1}^{(m)} = \frac{1}{P} \sum_{t=1}^P \mathbf{w}_t^{(m)\top} \mathbf{r}_{t+1}, \quad (44)$$

where \mathbf{r}_t is an $N \times 1$ vector of realised asset returns, P is the total out-of-sample length, and $\mathbf{w}_t^{(m)}$ are the portfolio weights at the start of period t for model m .

We focus on two main metrics to compare forecast models: out-of-sample portfolio *variance* and *turnover*. The variance of daily returns by a portfolio constructed by model m is:

$$\sigma_m^2 = \frac{1}{P} \sum_{t=1}^P (r_t^{(m)} - \bar{r}^{(m)})^2 \quad (45)$$

where $r_t^{(m)}$ is the ex-post return of model m in period t , $\bar{r}^{(m)}$ and P is its mean and number of observations over the out-of-sample window. Meanwhile, the average turnover reflects how often the portfolio adjusts its weights:

$$\text{TO}_m = \frac{1}{P-1} \sum_{t=1}^{P-1} \|\mathbf{w}_{t+1}^{(m)} - \mathbf{w}_{t+}^{(m)}\|_1, \quad (46)$$

where $\mathbf{w}_{t+}^{(m)}$ are the portfolio weights of model m immediately before rebalancing at $t+1$, and $\|\cdot\|_1$ is the 1-norm. A higher turnover implies more frequent portfolio adjustments, potentially incurring greater trading costs (Kourtis, 2014).

We also include an equally weighted ($1/N$) portfolio, often cited for its simplicity and historically strong performance (DeMiguel et al., 2009). Although $1/N$ avoids estimation risk and typically maintains low turnover, it cannot adapt to shifting market correlations.

From Table 5, it is evident that the covariance forecasts provided by the *CAB* model strike a

competitive balance between risk reduction and turnover across all rebalancing horizons. Across daily, weekly, and monthly rebalancing horizons, *CAB* slightly trails the top daily performer, approaches the leading weekly method, and matches or surpasses most other approaches monthly, thus consistently ranking among the best-performing models. This robust performance does not come at the cost of excessive turnover, as *CAB*'s turnover measures remain moderate compared to methods that may obtain marginally lower variances only at the expense of frequent portfolio rebalancing (e.g., *NA*, *DCC*, *DCC^{NL}*).

Table 5 – performance of the global minimum variance portfolios constructed using the covariance forecasts from the 11 models under consideration plus the equal-weighted portfolio. The portfolios are compared based on their annualised out-of-sample standard deviation (σ_m) and average out-of-sample turnover (TO_m), respectively. Results for three different rebalancing frequencies are presented.

	Daily		Weekly		Monthly	
	σ_m^2	TO_m	σ_m^2	TO_m	σ_m^2	TO_m
<i>1/N</i>	0.018132	0.005733	0.018115	0.002567	0.018060	0.001282
<i>NA</i>	0.001991	0.125568	0.002527	0.055395	0.002631	0.025707
<i>NA^F</i>	0.002451	0.001445	0.002453	0.000653	0.002461	0.000369
<i>EWMA</i>	0.002475	0.079388	0.002482	0.037928	0.002554	0.016088
<i>LW</i>	0.002655	0.098020	0.003373	0.047089	0.003598	0.022957
<i>LW^F</i>	0.002774	<u>0.001816</u>	0.002777	<u>0.000956</u>	0.002784	<u>0.000620</u>
<i>CCC</i>	0.002281	0.126519	0.002580	0.049839	0.002713	0.014816
<i>DCC</i>	0.002075	0.116446	0.002388	0.051710	<u>0.002524</u>	0.017159
<i>DCC^{NL}</i>	0.002048	0.129453	0.002448	0.056173	0.002618	0.023470
<i>PCA</i>	0.002680	0.197322	0.002722	0.072903	0.002657	0.023108
<i>RMT</i>	0.002647	0.125512	0.002689	0.055954	0.002733	0.024767
<i>CAB</i>	<u>0.002293</u>	0.078799	<u>0.002428</u>	0.048383	0.002579	0.023807

When compared to the $1/N$ benchmark, please note that all models present a statistically significant lower annual variance, based on the one-side F-Test of equalities of variance.

Examining the same metrics across distinct market regimes (Table A4) reveals that *CAB* remains a robust contender under varying conditions: in Bull-1, it consistently competes for the lowest variance, even attaining the best performance in weekly and monthly rebalancing; in the Bear regime, *CAB* ranks near the top in daily and weekly horizons, balancing lower turnover against marginally higher volatility than a few dynamic methods; and while Bull-2 sees other estimators occasionally surpass *CAB*, it still demonstrates stable risk control with moderate trading activity,

indicating that its effectiveness persists across both tranquil and turbulent market environments.

Comparisons to the $1/N$ benchmark further highlight the importance of adaptivity. While $1/N$ offers minimal turnover, it endures noticeably higher variance in all market conditions, reflecting its inability to exploit up-to-date correlation information. Indeed, the difference in annualised variances between CAB and $1/N$ can reach 80-90 basis points in certain scenarios, a gap that can substantially affect risk-adjusted returns and capital preservation.

Overall, CAB tends to exhibit moderate turnover, balancing the need to adjust to changing correlations without incurring unnecessary trades. This stability benefits investors who must limit transaction costs or adhere to regulatory constraints on turnover. These results underscore that advanced covariance estimation can yield *economically meaningful* improvements in risk control, particularly over the medium-term horizons favoured by many institutional investors. The CAB model stands out by combining strong variance reduction with stable rebalancing behaviour, balancing responsiveness to market changes and turnover efficiency.

6 Conclusion

We propose a novel DL framework for medium-term covariance forecasting in multi-asset portfolios, combining 3D convolutions, bidirectional LSTMs, and multi-head attention. Empirical tests on various ETFs from 2017 to 2023 reveal that this model, enhanced by a final shrinkage step, consistently outperforms classical benchmarks across different forecast horizons and market regimes.

Notably, its performance advantage remains robust whether one subtracts a risk-free rate from returns, suggesting broad applicability in diverse portfolio management practices.

In portfolio experiments, the proposed method enables global minimum-variance (GMV) strategies to achieve lower out-of-sample volatility with moderate turnover, underlining the tangible economic value of improved covariance estimation. By bridging cutting-edge DL techniques with established financial principles, our work highlights the promise of sophisticated spatiotemporal modelling for risk management and allocation decisions, especially at horizons where structural shifts and evolving correlations pose unique forecasting challenges.

Still, several research avenues warrant further exploration. First, extending the network architecture to accommodate skewed or heavy-tailed distributions could better capture tail risk in times of market stress. Second, explicitly incorporating transaction costs or liquidity constraints within the optimisation process might yield more realistic and implementable trading strategies. Finally,

evaluating the model in larger cross-sectional settings or applied to alternative asset classes (e.g., commodities, crypto assets) would illuminate its scalability and robustness.

We hope these findings encourage the finance community to explore and adapt advanced neural architectures for medium-term and long-horizon applications, strengthening the link between machine learning innovation and effective real-world asset allocation.

References

- Akiba, T., Sano, S., Yanase, T., Ohta, T., and Koyama, M. (2019). Optuna: A next-generation hyperparameter optimization framework. In *Proceedings of the 25th ACM SIGKDD International Conference on Knowledge Discovery & Data Mining*, pages 2623–2631. ACM. [3](#)
- Baillie, R. T. and Bollerslev, T. (1992). Prediction in dynamic models with time-dependent conditional variances. *Journal of Econometrics*, 52(1):91–113. [2.6](#)
- Bollerslev, T. (1990). Modelling the coherence in short-run nominal exchange rates: A multivariate generalized arch model. *The Review of Economics and Statistics*, 72(3):498–505. [1](#), [2.6](#)
- Bollerslev, T., Patton, A. J., and Quaedvlieg, R. (2018). Modeling and forecasting (un)reliable realized covariances for more reliable financial decisions. *Journal of Econometrics*, 207(1):71–91. [1](#), [2.12](#)
- Chiriac, R. and Voev, V. (2011). Modelling and forecasting multivariate realized volatility. *Journal of Applied Econometrics*, 26(6):922–947. [1](#)
- Cont, R. (2001). Empirical properties of asset returns: stylized facts and statistical issues. *Quantitative Finance*, 1(2):223. [2](#)
- Corsi, F. (2009). A simple approximate long-memory model of realized volatility. *Journal of Financial Econometrics*, 7(2):174–196. [1](#)
- De Nard, G., Engle, R. F., Ledoit, O., and Wolf, M. (2022). Large dynamic covariance matrices: Enhancements based on intraday data. *Journal of Banking & Finance*, 138:106426. [1](#), [2.6](#), [2.8](#)

- De Nard, G., Ledoit, O., and Wolf, M. (2021). Factor models for portfolio selection in large dimensions: The good, the better and the ugly. *Journal of Financial Econometrics*, 19(2):236–257. [1](#), [2.6](#)
- De Nard, G., Ledoit, O., and Wolf, M. (2024). Improved tracking-error management for active and passive investing. *Available at SSRN 4898624*. [1](#)
- DeMiguel, V., Garlappi, L., Nogales, F. J., and Uppal, R. (2009). A generalized approach to portfolio optimization: Improving performance by constraining portfolio norms. *Management Science*, 55:798–812. [5](#), [5](#)
- Demsar, J. (2006). Statistical comparisons of classifiers over multiple data sets. *J. Mach. Learn. Res.*, 7:1–30. [3](#)
- Elton, E. J. and Gruber, M. J. (1973). Estimating the dependence structure of share prices—implications for portfolio selection. *The Journal of Finance*, 28(5):1203–1232. [1](#)
- Engle, R. (2002). Dynamic conditional correlation. *Journal of Business & Economic Statistics*, 20(3):339–350. [1](#), [2.7](#)
- Engle, R. F. and Sheppard, K. (2001). Theoretical and empirical properties of dynamic conditional correlation multivariate garch. Working Paper 8554, National Bureau of Economic Research. [2.7](#)
- Gu, S., Kelly, B., and Xiu, D. (2020). Empirical asset pricing via machine learning. *The Review of Financial Studies*, 33:2223–2273. [1](#)
- Hansen, B. E. (1994). Autoregressive conditional density estimation. *International Economic Review*, 35(3):705–730. [2](#)
- Harvey, A. (1997). Trends, cycles and autoregressions. *The Economic Journal*, 107(440):192–201. [2](#)
- Hochreiter, S. (1997). Long short-term memory. *Neural Computation MIT-Press*. [2.11.3](#), [A.1](#)
- J.P.Morgan (1996). *Riskmetrics technical document*. Morgan Guaranty Trust Company of New York. [2.3](#)

- Kim, I., Lee, M., and Seok, J. (2023). Icegan: inverse covariance estimating generative adversarial network. *Machine Learning: Science and Technology*, 4:025008. [1](#)
- Kourtis, A. (2014). On the distribution and estimation of trading costs. *Journal of Empirical Finance*, 28:104–117. [5](#)
- Kourtis, A., Dotsis, G., and Markellos, R. N. (2012). Parameter uncertainty in portfolio selection: Shrinking the inverse covariance matrix. *Journal of Banking & Finance*, 36(9):2522–2531. [5](#)
- Laloux, L., Cizeau, P., Potters, M., and Bouchaud, J.-P. (2000). Random matrix theory and financial correlations. *International Journal of Theoretical and Applied Finance*, 03:391–397. [1](#), [2.10](#)
- Lecun, Y., Bottou, L., Bengio, Y., and Haffner, P. (1998). Gradient-based learning applied to document recognition. *Proceedings of the IEEE*, 86(11):2278–2324. [2.11.2](#)
- Ledoit, O. and Wolf, M. (2003). Improved estimation of the covariance matrix of stock returns with an application to portfolio selection. *Journal of Empirical Finance*, 10(5):603–621. [1](#), [2.9](#)
- Ledoit, O. and Wolf, M. (2004). A well-conditioned estimator for large-dimensional covariance matrices. *Journal of Multivariate Analysis*, 88(2):365–411. [1](#), [2.4](#), [2.5](#)
- Ledoit, O. and Wolf, M. (2020). Analytical nonlinear shrinkage of large-dimensional covariance matrices. *The Annals of Statistics*, 48(5):3043 – 3065. [2.8](#)
- Ledoit, O. and Wolf, M. (2022). The power of (non-)linear shrinking: A review and guide to covariance matrix estimation. *Journal of Financial Econometrics*, 20:187–218. [1](#)
- Liu, G. and Guo, J. (2019). Bidirectional lstm with attention mechanism and convolutional layer for text classification. *Neurocomputing*, 337:325–338. [2.11.3](#)
- Markowitz, H. (1952). Portfolio selection. *The Journal of Finance*, 7:77–91. [1](#), [4.1](#)
- Nazareth, N. and Ramana Reddy, Y. V. (2023). Financial applications of machine learning: A literature review. *Expert Systems with Applications*, 219:119640. [1](#)
- Olorunnimbe, K. and Viktor, H. (2023). Deep learning in the stock market—a systematic survey of practice, backtesting, and applications. *Artificial Intelligence Review*, 56(3):2057–2109. [1](#)

- Reis, P., Serra, A. P., and Gama, J. (2024). The role of deep learning in financial asset management: A systematic review. *Authorea, Inc.* [1](#)
- Robert F. Engle, O. L. and Wolf, M. (2019). Large dynamic covariance matrices. *Journal of Business & Economic Statistics*, 37(2):363–375. [1](#)
- Sandoval, L. and Franca, I. D. P. (2012). Correlation of financial markets in times of crisis. *Physica A: Statistical Mechanics and its Applications*, 391(1):187–208. [1](#)
- Symitsi, E., Symeonidis, L., Kourtis, A., and Markellos, R. (2018). Covariance forecasting in equity markets. *Journal of Banking & Finance*, 96:153–168. [1](#), [2.12](#), [5](#)
- Vaswani, A., Shazeer, N. M., Parmar, N., Uszkoreit, J., Jones, L., Gomez, A. N., Kaiser, L., and Polosukhin, I. (2017). Attention is all you need. In *Neural Information Processing Systems*. [1](#), [2.11.4](#)
- Zhang, C., Pu, X., Cucuringu, M., and Dong, X. (2024). Graph-based methods for forecasting realized covariances. *Journal of Financial Econometrics*, page nbae026. [1](#), [2.12](#)

A Appendix

A.1 LSTM cell detailed explanation

An LSTM (Hochreiter, 1997) cell consists of three main gates: the forget gate (f_t), the input gate (i_t), and the output gate (o_t). They are respectively calculated as:

$$f_t = \sigma(\mathbf{W}_f \cdot [\mathbf{h}_{(t-1)}, \mathbf{x}_t] + \mathbf{b}_f) \quad (\text{A.1})$$

$$i_t = \sigma(\mathbf{W}_i \cdot [\mathbf{h}_{(t-1)}, \mathbf{x}_t] + \mathbf{b}_i) \quad (\text{A.2})$$

$$o_t = \sigma(\mathbf{W}_o \cdot [\mathbf{h}_{(t-1)}, \mathbf{x}_t] + \mathbf{b}_o) \quad (\text{A.3})$$

where \mathbf{x}_t is the vector input at time t , $\mathbf{h}_{(t-1)}$ is the hidden vector state, \mathbf{W}_f , \mathbf{W}_i and \mathbf{W}_c are weight matrices, and \mathbf{b}_f , \mathbf{b}_i and \mathbf{b}_o are bias vectors. The sigmoid function σ ensures that the output values are between 0 and 1, representing how much each component should be forgotten.

The forget gate decides what information should be discarded from the cell state. Next, the input gate determines what new information should be added to the cell state. This process involves two steps: calculating the input gate Eq. (A.2) and creating new candidate values:

$$\tilde{\mathbf{C}}_t = \tanh(\mathbf{W}_c \cdot [\mathbf{h}_{t-1}, \mathbf{x}_t] + \mathbf{b}_c) \quad (\text{A.4})$$

where \mathbf{W}_c is the weight matrix, and \mathbf{b}_c is a bias vector. The input gate modulates the extent to which new information is added to the cell state. The cell state update combines the forget gate and input gate operations to update the cell state:

$$\mathbf{C}_t = f_t \odot \mathbf{C}(t-1) + i_t \odot \tilde{\mathbf{C}}_t \quad (\text{A.5})$$

This equation ensures that the cell state retains essential information over long periods.

Finally, the output gate controls what information should be outputted from the cell. This involves two steps: calculating the output gate Eq. (A.3) and determining the hidden state:

$$\mathbf{h}_t = o_t \odot \tanh(\mathbf{C}_t) \quad (\text{A.6})$$

A.2 Hyperparameter Grid Search

Table A1 – Hyperparameter Grid Search table.

Hyperparameter	Range
Optimiser	Adam, SGD
Batch size	32, 64, 128, 256
Learning rate	10^{-3} , 10^{-4} , 10^{-5}
Lookback window (L)	20, 40, 60, 80, 100, 120, 250
3D convolution kernel size (ks)	3, 5, 7
BiLSTM hidden dimensions (hd)	32, 64, 128, 256
BiLSTM stacked layers (u)	3, 4, 5, 6, 7
Number of heads (he) ^a	2, 4, 6, 8, 16, 32
Shrinkage factor (ϕ)	0.00, 0.20, 0.40, 0.60, 0.80, 1.00

A.3 Extended Data Tables

Table A2 – Average Euclidean (\mathcal{L}^E) and Frobenius (\mathcal{L}^F) distances ($\times 10^5$) using *excess* returns with different horizons (F) for different testing periods: Overall (1 January 2021 to 31 December 2023), Bull-1 (1 January 2021 to 2 January 2022), Bear (3 January 2022 to 12 June 2022), and Bull-2 (13 June 2022 to 31 December 2023).

	Overall		Bull-1		Bear		Bull-2	
	\mathcal{L}^E	\mathcal{L}^F	\mathcal{L}^E	\mathcal{L}^F	\mathcal{L}^E	\mathcal{L}^F	\mathcal{L}^E	\mathcal{L}^F
NA	70.309	107.739	54.194	82.600	107.447	165.092	69.960	107.363
NA^F	62.260	95.586	46.956	71.921	106.652	163.471	59.271	91.185
$EWMA$	58.851	90.253	42.125	64.612	<u>94.704</u>	145.253	59.272	90.889
LW	63.548	97.681	47.376	72.757	104.804	160.926	62.036	95.449
LW^F	75.861	115.370	69.194	104.027	105.832	162.356	71.461	109.054
CCC	<u>58.111</u>	<u>89.824</u>	<u>42.451</u>	<u>65.818</u>	95.819	147.003	<u>57.301</u>	<u>88.763</u>
DCC	62.210	95.018	48.557	73.797	96.913	147.989	60.972	93.374
DCC^{NL}	65.361	99.154	51.461	77.640	100.48	152.649	64.160	97.548
PCA	71.266	109.164	54.984	83.752	110.811	170.301	70.323	107.864
RMT	71.064	108.951	54.819	83.588	110.623	170.011	70.094	107.641

Continued on next page

	\mathcal{L}^E	\mathcal{L}^F	\mathcal{L}^E	\mathcal{L}^F	\mathcal{L}^E	\mathcal{L}^F	\mathcal{L}^E	\mathcal{L}^F
<i>CAB</i>	56.954	87.317	44.134	67.401	94.689	<u>145.287</u>	54.291	83.369
<i>NA</i>	45.872	70.272	24.755	38.850	<u>72.135</u>	<u>108.838</u>	51.939	79.449
<i>NA^F</i>	47.436	72.906	31.056	47.811	90.540	139.813	45.522	69.719
<i>EWMA</i>	44.734	68.528	26.175	40.546	74.009	112.405	48.262	73.923
<i>LW</i>	43.441	66.728	<u>23.834</u>	<u>37.275</u>	76.162	114.702	46.645	71.886
<i>LW^F</i>	63.848	96.730	62.374	93.125	78.628	122.264	60.501	91.635
<i>CCC</i>	43.434	67.183	27.608	43.493	75.190	114.891	44.465	68.675
<i>DCC</i>	<u>42.622</u>	<u>66.124</u>	27.194	42.996	73.983	113.348	<u>43.509</u>	<u>67.391</u>
<i>DCC^{NL}</i>	43.764	67.604	28.135	44.201	75.173	114.919	44.767	69.024
<i>PCA</i>	46.390	71.007	24.934	39.238	72.294	109.567	52.781	80.410
<i>RMT</i>	46.177	70.771	24.796	39.028	72.411	109.269	52.424	80.176
<i>CAB</i>	22.851	35.411	13.091	20.268	42.372	65.754	23.505	36.408
<i>NA</i>	44.053	68.114	26.115	42.593	72.110	109.681	47.531	72.584
<i>NA^F</i>	45.519	69.961	30.907	47.659	83.084	128.667	44.068	67.348
<i>EWMA</i>	44.704	68.490	26.626	41.728	74.557	112.995	47.751	72.910
<i>LW</i>	42.035	65.084	<u>24.836</u>	<u>40.385</u>	75.018	113.948	43.600	66.895
<i>LW^F</i>	62.001	93.989	62.649	93.590	69.286	108.383	59.458	90.055
<i>CCC</i>	42.647	66.037	29.089	45.917	<u>68.525</u>	<u>105.242</u>	43.916	67.686
<i>DCC</i>	<u>40.986</u>	<u>63.934</u>	26.426	42.585	69.459	106.517	<u>42.150</u>	<u>65.398</u>
<i>DCC^{NL}</i>	42.268	65.595	27.106	43.443	71.582	109.283	43.579	67.259
<i>PCA</i>	44.550	68.801	26.466	43.142	72.705	111.010	48.096	73.173
<i>RMT</i>	44.334	68.575	26.291	42.936	72.803	110.768	47.761	72.940
<i>CAB</i>	22.305	34.990	12.842	20.226	39.166	62.879	23.540	36.458
<i>NA</i>	43.972	68.530	30.179	49.646	76.424	117.032	43.479	66.670
<i>NA^F</i>	43.572	67.004	30.527	47.207	83.143	128.419	40.520	<u>61.975</u>

Continued on next page

	\mathcal{L}^E	\mathcal{L}^F	\mathcal{L}^E	\mathcal{L}^F	\mathcal{L}^E	\mathcal{L}^F	\mathcal{L}^E	\mathcal{L}^F	
$F = 90$	<i>EWMA</i>	44.720	68.781	28.925	<u>45.742</u>	73.402	111.890	46.624	71.190
	<i>LW</i>	42.446	66.204	<u>28.694</u>	47.283	79.704	121.665	40.527	62.340
	<i>LW^F</i>	60.006	91.073	61.704	92.289	<u>64.055</u>	<u>100.713</u>	57.724	87.477
	<i>CCC</i>	43.390	67.342	32.735	51.757	68.495	105.076	42.999	66.475
	<i>DCC</i>	<u>40.234</u>	<u>63.342</u>	29.961	48.303	65.688	101.473	<u>39.492</u>	62.005
	<i>DCC^{NL}</i>	42.615	66.462	29.762	48.148	71.380	108.855	42.584	66.011
	<i>PCA</i>	44.464	69.171	30.520	50.091	76.867	118.267	44.085	67.265
	<i>RMT</i>	44.239	68.951	30.343	49.925	77.105	118.060	43.693	67.005
	<i>CAB</i>	13.977	21.752	10.080	16.184	20.742	32.133	14.538	22.346
$F = 120$	<i>NA</i>	48.590	<u>75.398</u>	<u>36.397</u>	<u>59.019</u>	84.342	128.425	<u>46.097</u>	<u>70.593</u>
	<i>NA^F</i>	41.909	64.465	31.713	49.127	84.615	129.958	36.093	55.352
	<i>EWMA</i>	45.330	69.861	33.556	53.195	71.953	109.497	45.222	69.142
	<i>LW</i>	47.098	73.175	34.956	56.786	87.296	132.635	43.277	66.502
	<i>LW^F</i>	58.216	88.420	60.114	90.286	<u>64.569</u>	<u>100.736</u>	55.133	83.621
	<i>CCC</i>	44.163	68.631	36.440	57.692	71.518	108.718	41.212	64.060
	<i>DCC</i>	<u>40.946</u>	64.563	33.741	54.358	68.094	104.261	37.719	59.629
	<i>DCC^{NL}</i>	44.082	68.671	34.120	54.937	74.174	112.239	41.789	64.902
	<i>PCA</i>	49.115	76.015	36.715	59.374	84.740	129.651	46.794	71.202
<i>RMT</i>	48.867	75.827	36.519	59.220	85.041	129.486	46.352	70.985	
<i>CAB</i>	12.635	19.816	10.718	17.319	18.659	29.190	12.125	18.707	
$F = 180$	<i>NA</i>	57.475	88.882	50.083	79.438	92.682	140.191	52.022	80.073
	<i>NA^F</i>	<u>38.460</u>	<u>59.180</u>	<u>32.171</u>	<u>49.910</u>	82.117	124.805	<u>29.829</u>	<u>46.088</u>
	<i>EWMA</i>	50.035	77.019	43.437	68.307	76.903	116.122	46.487	71.288
	<i>LW</i>	56.137	86.937	49.005	77.757	94.604	142.932	49.567	76.591
	<i>LW^F</i>	54.308	82.570	54.261	81.972	<u>45.646</u>	<u>95.111</u>	52.187	79.306
	<i>CCC</i>	44.949	70.232	40.531	64.242	72.901	110.150	39.678	62.498
	<i>DCC</i>	46.528	72.381	41.217	65.244	75.945	114.305	41.410	64.807
<i>DCC^{NL}</i>	46.532	72.386	41.220	65.248	75.950	114.312	41.414	64.812	

Continued on next page

	\mathcal{L}^E	\mathcal{L}^F	\mathcal{L}^E	\mathcal{L}^F	\mathcal{L}^E	\mathcal{L}^F	\mathcal{L}^E	\mathcal{L}^F
<i>PCA</i>	58.026	89.446	50.494	79.976	92.884	141.079	52.765	80.559
<i>RMT</i>	57.744	89.294	50.351	79.843	93.189	140.964	52.223	80.384
<i>CAB</i>	12.356	19.146	11.116	17.602	18.159	27.468	11.472	17.726
<i>NA</i>	76.850	117.44	107.237	163.541	79.505	120.16	56.341	86.706
<i>NA^F</i>	<u>34.002</u>	<u>52.367</u>	<u>33.076</u>	<u>51.123</u>	64.126	97.309	25.830	<u>40.087</u>
<i>EWMA</i>	53.737	82.720	53.030	82.554	72.648	109.762	48.689	74.953
<i>LW</i>	74.903	114.697	103.984	158.986	80.825	122.029	54.291	83.797
<i>LW^F</i>	49.653	75.499	47.293	71.542	<u>45.646</u>	<u>70.522</u>	52.353	79.519
<i>CCC</i>	43.487	68.479	42.628	67.459	58.966	89.895	39.537	62.904
<i>DCC</i>	40.299	64.494	38.892	62.869	53.375	82.622	37.405	60.269
<i>DCC^{NL}</i>	40.223	66.604	49.514	77.717	81.610	120.697	<u>22.135</u>	43.633
<i>PCA</i>	77.628	118.284	108.476	165.211	79.544	120.791	57.035	87.075
<i>RMT</i>	77.315	118.139	108.26	165.074	79.841	120.668	56.481	86.919
<i>CAB</i>	16.116	24.758	22.511	34.543	16.201	24.572	11.938	18.457

F = 250

Table A3 – Average Euclidean (\mathcal{L}^E) and Frobenius (\mathcal{L}^F) distances ($\times 10^5$) using *raw* returns with different horizons (F) for different testing periods: Overall (1 January 2021 to 31 December 2023), Bull-1 (1 January 2021 to 2 January 2022), Bear (3 January 2022 to 12 June 2022), and Bull-2 (13 June 2022 to 31 December 2023).

	Overall		Bull-1		Bear		Bull-2	
	\mathcal{L}^E	\mathcal{L}^F	\mathcal{L}^E	\mathcal{L}^F	\mathcal{L}^E	\mathcal{L}^F	\mathcal{L}^E	\mathcal{L}^F
$F = 10$								
<i>NA</i>	70.309	107.739	54.193	82.599	107.449	165.094	69.959	107.362
<i>NA^F</i>	62.057	95.297	46.340	71.028	107.068	164.102	59.155	91.020
<i>EWMA</i>	58.908	90.338	42.125	64.612	<u>94.704</u>	<u>145.253</u>	59.384	91.053
<i>LW</i>	63.547	97.680	47.376	72.755	104.804	160.927	62.035	95.448
<i>LW^F</i>	75.854	115.361	69.181	104.007	105.831	162.355	71.457	109.048
<i>CCC</i>	58.092	<u>89.783</u>	<u>42.384</u>	<u>65.733</u>	95.843	147.035	57.300	88.730
<i>DCC</i>	62.186	94.973	48.470	73.686	96.894	147.968	60.986	93.364
<i>DCC^{NL}</i>	65.338	99.111	51.367	77.516	100.447	152.608	64.186	97.557
<i>PCA</i>	71.265	109.164	54.983	83.750	110.813	170.304	70.322	107.863
<i>RMT</i>	71.064	108.951	54.818	83.587	110.625	170.014	70.093	107.640
<i>CAB</i>	<u>58.272</u>	89.475	43.967	67.109	94.554	145.032	56.996	87.822
$F = 40$								
<i>NA</i>	45.876	70.278	24.754	38.850	<u>72.131</u>	<u>108.833</u>	51.948	79.462
<i>NA^F</i>	47.200	72.577	30.161	46.526	91.426	141.121	45.386	69.534
<i>EWMA</i>	44.796	68.618	26.174	40.545	74.005	112.399	48.383	74.100
<i>LW</i>	43.444	66.733	<u>23.834</u>	<u>37.275</u>	76.161	114.700	46.652	71.896
<i>LW^F</i>	63.845	96.725	62.359	93.102	78.638	122.279	60.502	91.636
<i>CCC</i>	43.321	67.023	27.469	43.276	75.123	114.858	44.354	68.515
<i>DCC</i>	<u>42.585</u>	<u>66.060</u>	27.081	42.811	74.082	113.527	<u>43.481</u>	<u>67.335</u>
<i>DCC^{NL}</i>	43.739	67.556	28.016	44.008	75.278	115.106	44.766	69.003
<i>PCA</i>	46.394	71.012	24.934	39.237	72.291	109.562	52.789	80.423
<i>RMT</i>	46.181	70.777	24.796	39.027	72.408	109.265	52.432	80.188
<i>CAB</i>	26.619	41.417	13.427	20.765	45.197	69.510	29.777	46.649

Continued on next page

	\mathcal{L}^E	\mathcal{L}^F	\mathcal{L}^E	\mathcal{L}^F	\mathcal{L}^E	\mathcal{L}^F	\mathcal{L}^E	\mathcal{L}^F	
$F = 60$	NA	44.060	68.125	26.115	42.593	72.109	109.679	47.545	72.605
	NA ^F	45.268	69.612	30.016	46.385	84.049	130.081	43.879	67.086
	EWMA	44.759	68.570	26.625	41.727	74.548	112.981	47.861	73.069
	LW	42.043	65.095	<u>24.836</u>	<u>40.385</u>	75.020	113.951	43.615	66.916
	LW ^F	62.000	93.988	62.634	93.568	69.301	108.405	59.462	90.061
	CCC	42.543	65.895	28.943	45.693	68.234	104.807	43.895	67.683
	DCC	<u>39.404</u>	<u>61.909</u>	26.764	42.978	<u>64.589</u>	<u>100.135</u>	<u>40.279</u>	<u>63.072</u>
	DCC ^{NL}	42.240	65.544	27.015	43.295	71.326	108.855	43.658	67.380
	PCA	44.557	68.811	26.466	43.142	72.705	111.009	48.109	73.194
	RMT	44.341	68.586	26.291	42.935	72.803	110.767	47.775	72.961
CAB	24.079	37.328	13.698	21.649	43.977	68.513	25.026	38.428	
$F = 90$	NA	43.982	68.545	30.179	49.646	76.435	117.049	43.496	66.694
	NA ^F	43.314	66.645	29.713	46.043	84.231	130.003	40.232	<u>61.574</u>
	EWMA	44.761	68.841	28.925	<u>45.742</u>	73.405	111.893	46.704	71.306
	LW	42.457	66.219	<u>28.694</u>	47.283	79.715	121.682	40.544	62.365
	LW ^F	60.007	91.075	61.690	92.268	<u>64.073</u>	<u>100.740</u>	57.731	87.486
	CCC	43.276	67.199	32.551	51.513	68.021	104.421	43.036	66.546
	DCC	<u>40.134</u>	<u>63.219</u>	29.870	48.186	65.191	100.793	<u>39.503</u>	62.039
	DCC ^{NL}	42.532	66.357	29.680	48.045	70.880	108.147	42.622	66.080
	PCA	44.474	69.186	30.520	50.092	76.878	118.284	44.100	67.288
	RMT	44.249	68.966	30.343	49.925	77.116	118.077	43.709	67.029
CAB	14.661	23.076	10.115	16.203	22.040	34.086	15.465	24.333	
$F = 120$	NA	48.604	75.417	36.397	59.018	84.366	128.460	46.116	70.620
	NA ^F	<u>41.664</u>	<u>64.124</u>	<u>31.048</u>	<u>48.181</u>	85.754	131.620	<u>35.717</u>	<u>54.821</u>
	EWMA	45.361	69.908	33.555	53.194	71.959	109.504	45.282	69.232
	LW	47.111	73.194	34.955	56.785	87.320	132.670	43.296	66.530
	LW ^F	58.219	88.425	60.101	90.267	<u>64.599</u>	<u>100.781</u>	55.138	83.629
	CCC	44.126	68.610	36.335	57.587	71.120	108.182	41.325	64.245

Continued on next page

		\mathcal{L}^E	\mathcal{L}^F	\mathcal{L}^E	\mathcal{L}^F	\mathcal{L}^E	\mathcal{L}^F	\mathcal{L}^E	\mathcal{L}^F
$F = 120$	<i>DCC</i>	43.988	68.569	34.032	54.862	73.636	111.512	41.819	64.965
	<i>DCC^{NL}</i>	44.025	68.619	34.051	54.887	73.690	111.582	41.864	65.025
	<i>PCA</i>	49.129	76.034	36.715	59.373	84.764	129.686	46.813	71.230
	<i>RMT</i>	48.881	75.846	36.519	59.219	85.065	129.521	46.371	71.013
	<i>CAB</i>	12.118	18.831	9.496	15.248	17.864	27.435	12.147	18.653
$F = 180$	<i>NA</i>	57.494	88.910	50.085	79.441	92.730	140.261	52.044	80.105
	<i>NA^F</i>	<u>38.294</u>	<u>58.953</u>	<u>31.839</u>	<u>49.444</u>	83.328	126.577	<u>29.370</u>	<u>45.434</u>
	<i>EWMA</i>	50.062	77.060	43.438	68.309	76.943	116.140	46.536	71.363
	<i>LW</i>	56.156	86.964	49.007	77.759	94.651	143.001	49.589	76.623
	<i>LW^F</i>	54.314	82.579	54.255	81.962	<u>61.748</u>	<u>95.188</u>	52.188	79.307
	<i>CCC</i>	44.844	70.073	40.368	64.069	72.299	109.109	39.755	62.603
	<i>DCC</i>	46.364	72.137	41.041	65.057	75.312	113.195	41.391	64.777
	<i>DCC^{NL}</i>	46.406	72.191	41.077	65.104	75.366	113.267	41.432	64.830
	<i>PCA</i>	58.045	89.474	50.496	79.979	92.932	141.148	52.787	80.592
	<i>RMT</i>	57.763	89.322	50.352	79.846	93.237	141.034	52.245	80.416
<i>CAB</i>	12.828	19.854	11.180	17.728	20.372	30.851	11.702	18.031	
$F = 250$	<i>NA</i>	76.900	117.511	107.237	163.540	79.568	120.252	56.420	86.818
	<i>NA^F</i>	<u>34.000</u>	<u>52.376</u>	<u>33.222</u>	<u>51.351</u>	65.353	99.107	25.373	<u>39.432</u>
	<i>EWMA</i>	53.792	82.799	53.034	82.561	72.673	109.796	48.785	75.090
	<i>LW</i>	74.952	114.767	103.983	158.985	80.888	122.122	54.369	83.906
	<i>LW^F</i>	49.692	75.555	47.295	71.544	<u>45.710</u>	<u>70.616</u>	52.408	79.599
	<i>CCC</i>	43.349	68.233	42.431	67.189	58.278	88.611	39.597	62.977
	<i>DCC</i>	40.167	64.257	38.751	62.682	52.667	81.284	37.446	60.321
	<i>DCC^{NL}</i>	40.261	66.455	49.351	77.363	80.796	119.188	<u>22.552</u>	44.012
	<i>PCA</i>	77.678	118.355	108.475	165.210	79.607	120.884	57.115	87.187
	<i>RMT</i>	77.365	118.210	108.260	165.073	79.904	120.760	56.560	87.032
<i>CAB</i>	18.246	27.828	29.049	44.148	14.976	22.681	12.182	18.727	

Table A4 – Performance of the GMV portfolios constructed using the covariance forecasts from the 11 models under consideration plus the equal-weighted portfolio for the different market regimes. The portfolios are compared based on their annualised out-of-sample standard deviation (σ_m) and average out-of-sample turnover (TO_m), respectively.

	Daily		Weekly		Monthly		
	σ_m^2	TO_m	σ_m^2	TO_m	σ_m^2	TO_m	
Bull-1	1/N	0.009883	0.005169	0.009873	0.002335	0.009907	0.001103
	NA	0.000543	0.150112	0.000794	0.060372	0.000834	0.026885
	NA ^F	0.000731	<u>0.001378</u>	0.000732	0.000607	0.000736	0.000327
	EWMA	0.000735	0.088541	0.000748	0.043884	0.000754	0.015613
	LW	0.001054	0.091979	0.001572	0.044883	0.001692	0.022283
	LW ^F	0.000780	0.001228	0.000781	<u>0.000610</u>	0.000783	<u>0.000349</u>
	CCC	0.000620	0.119486	<u>0.000681</u>	0.053221	<u>0.000728</u>	0.013605
	DCC	<u>0.000529</u>	0.207262	0.000698	0.093558	0.000781	0.024324
	DCC ^{NL}	0.000522	0.217432	0.000784	0.097809	0.000875	0.034673
	PCA	0.000850	0.236835	0.000827	0.090803	0.000795	0.020906
	RMT	0.000856	0.150601	0.000860	0.067402	0.000826	0.025859
	CAB	0.000634	0.086489	0.000656	0.055931	0.000707	0.023736
Bear	1/N	0.029939	0.007221	0.029940	0.003443	0.029793	0.001599
	NA	0.002207	0.092111	0.002682	0.032018	0.002959	0.018142
	NA ^F	0.002891	0.001650	0.002892	0.000935	0.002906	0.000436
	EWMA	0.002908	0.079065	0.002843	0.036314	0.003120	0.019997
	LW	0.003118	0.095723	0.003970	0.041663	0.004754	0.021610
	LW ^F	0.003196	<u>0.002035</u>	0.003197	<u>0.001043</u>	0.003201	<u>0.000570</u>
	CCC	0.002497	0.129487	<u>0.002646</u>	0.043843	0.002590	0.012451
	DCC	0.002355	0.067768	0.002639	0.015372	<u>0.002636</u>	0.005911
	DCC ^{NL}	<u>0.002269</u>	0.083567	0.002652	0.024277	0.002730	0.010308
	PCA	0.002800	0.114256	0.002792	0.043637	0.002864	0.011111
	RMT	0.002983	0.094396	0.002896	0.037508	0.003153	0.023308
	CAB	0.002273	0.030506	0.002464	0.022686	0.002656	0.016836

Continued on next page

	Daily		Weekly		Monthly	
	σ_m^2	TO_m	σ_m^2	TO_m	σ_m^2	TO_m
$1/N$	0.019967	0.005666	0.019956	0.002382	0.019933	0.001334
NA	0.002823	0.118997	0.003526	0.053457	0.003667	0.029686
NA^F	0.003398	0.001426	0.003400	0.000577	0.003406	0.000261
$EWMA$	0.003432	0.073812	0.003433	0.034460	0.003630	0.016887
LW	0.003512	0.102531	0.004274	0.048313	0.004245	0.020765
LW^F	0.003874	<u>0.002113</u>	0.003879	<u>0.001123</u>	0.003889	<u>0.000788</u>
CCC	0.003233	0.129874	0.003635	0.047812	0.003671	0.015276
DCC	0.002947	0.071444	0.003294	0.026871	0.003364	0.009476
DCC^{NL}	<u>0.002924</u>	0.085242	<u>0.003318</u>	0.034070	<u>0.003365</u>	0.012661
PCA	0.003793	0.194898	0.003678	0.063899	0.003597	0.024379
RMT	0.003668	0.118539	0.003720	0.055498	0.003762	0.029837
CAB	0.003323	0.087821	0.003547	0.052596	0.003885	0.029487